Optics Letters

Dynamics of soliton molecules in a normal-dispersion fiber laser

JUNSONG PENG AND HEPING ZENG*

State Key Laboratory of Precision Spectroscopy, East China Normal University, Shanghai 200062, China
*Corresponding author: hpzeng@phy.ecnu.edu.cn

Received 20 March 2019; revised 3 May 2019; accepted 5 May 2019; posted 10 May 2019 (Doc. ID 362959); published 30 May 2019

Soliton molecules have been extensively investigated in mode-locked anomalous-dispersion fiber lasers by virtue of real-time measurement technologies. However, in the normal-dispersion regime, it is unclear how a soliton molecule evolves. Here, we first present, to the best of our knowledge, experimental investigations on the dynamics of soliton molecules in the normal-dispersion regime. We observe aperiodical evolutions of two dissipative solitons within a soliton molecule. They exchange energies during propagation. In particular, the large dissipative soliton splits when energy exchange occurs. Rogue waves are first revealed in the spectral domain of soliton molecules. High-resolution time-stretch technique, field autocorrelation analysis, and spatiotemporal intensity measurements allow us to reveal these critical behaviors of soliton molecules.

https://doi.org/10.1364/OL.44.002899

Using real-time measurement technologies, mode-locked lasers can now be characterized in a single-shot mode, which was previously impossible as standard measurement tools can only measure time-averaged data. By monitoring the outputs of mode-locked lasers in real-time using a time-stretch technique [1], a rich set of novel laser dynamics are revealed. For example, the build-up of mode locking in Ti: sapphire lasers was revealed [2]. Later on, the build-up of mode locking was also reported in fiber lasers [3,4]. In particular, it was found that the build-up dynamics of mode locking in fiber lasers depend crucially on the length of a laser cavity: a long cavity gives rise to transient soliton molecules during the build-up of mode locking while a shorter cavity resembles that of a Ti: Sapphire laser which does not generate transient soliton molecules [4]. Though Q-switching is generally present in the build-up of mode locking, such instability is suppressed during the build-up of mode locking using a carbon nanotube as a saturable absorber [5,6].

On the other hand, the internal dynamics of soliton molecules were probed by the time-stretch technique [7–10], leading to the discoveries of various soliton molecules, including vibrating soliton molecules [7,8] and intermittent vibrating soliton molecules [9]. The build-up of soliton molecules was also investigated to address a crucial question on how soliton molecules are formed from initial noise fluctuations in a laser [9]. It was found that double solitons are generated from the splitting of a large soliton, and they experience diverse interactions (depending on the initial noise) before forming a stationary soliton molecule.

The fast dynamics of soliton molecules have been exclusively studied in an anomalous dispersion regime. Mode-locked lasers in a normal dispersion regime, first demonstrated by Chong *et al.* [11], are superior over these in the anomalous dispersion regime in terms of pulse energy, quality, and duration [12], and they are ideal seed sources for chirped-pulse amplification [13]. Although soliton molecules were found in the normal dispersion regime, knowledge on their real-time dynamics was prevented from standard measurement tools [14]. A numerical study was performed to investigate the dynamics of soliton molecules in the normal dispersion regime [15]. Formation of soliton molecules is realized by the oscillating structures in soliton tails [16]. Such a binding mechanism was thoroughly demonstrated in experiments [17]. These oscillating tails are generated by Kelly sidebands in mode-locked anomalous dispersion lasers. In contrast, there are no Kelly sidebands in the normal dispersion regime, implying that the dynamics of soliton molecules could differ.

Here, we first investigate real-time measurements of soliton molecules in a mode-locked normal-dispersion fiber laser. The time-stretch dispersive Fourier transformation (TS-DFT) technique with a high resolution is used to measure the round-trip resolved spectra and a field autocorrelation analysis is employed to reveal the temporal evolutions assisted by spatiotemporal intensity measurements. The separation between two bound dissipative solitons (DSs) evolves aperiodically. An additional modulation on the spectra is observed suggesting that the DSs split aperiodically. Such a splitting occurs when the DSs exchange energy. Moreover, rogue waves are present in the soliton molecule. No stationary soliton molecules are found in the experiment.

The laser setup is illustrated in Fig. 1(a). A piece of erbium-doped fiber (EDF, OFS80) is used as a gain medium which is pumped by a 980-nm laser diode. Mode locking is realized by nonlinear polarization rotation, which consists of two polarization controllers sandwiched by a polarization dependent isolator. Setting the polarization controllers in proper positions, mode locking can be achieved. To manage the net dispersion

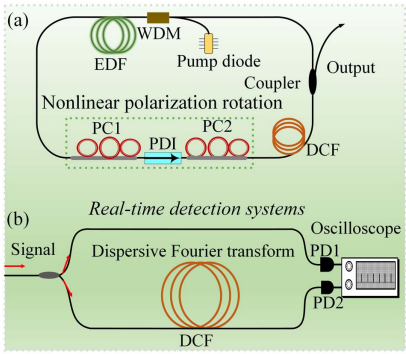

Fig. 1. (a) Laser setup. (b) Detection system.

of the laser to be normal, a piece of dispersion-compensating fiber (DCF38) which has normal dispersion at 1550 nm is employed in the cavity. The net dispersion of the laser is 0.0037 ps^2. The total cavity length is 11.5 m. As shown in Fig. 1(b), the output of the laser is delivered to a coupler which splits the signal to two ports. One is for temporal intensity measurement and the other is to implement TS-DFT via a long piece of DCF.

A rich set of laser dynamics has been observed in mode-locked normal-dispersion fiber lasers by virtue of TS-DFT including soliton explosions [18–23], dual-color soliton collisions [24], as well as rogue waves [25,26] and triple-state dissipative soliton switching [27]. Here, soliton molecule dynamics are studied. Under single-pulse mode locking, the pulse has a duration of 16.2 ps with a 3 dB spectral width of 9 nm. The corresponding time-bandwidth product is 18, meaning the pulse is highly chirped. To generate soliton molecules, the laser was operated under a pump power of 237 mW, far from the mode-locking threshold (133 mW). Soliton molecules were observed under this pump power. Rotating the polarization controllers made the laser transfer to noise-like pulsing. This work focuses on the regime of soliton molecules. Figure 2(a) shows the TS-DFT measured spectra of soliton molecules. Figure 2(b) shows the temporal dynamics revealed by the field autocorrelation trace which is calculated by Fourier transformations of Fig. 2(a) [4,7,9,19]. Two pulses yield three peaks in the autocorrelation traces. The distance between the central peak and the left or the right peak refers to the temporal separation between bound DSs. Figure 2(c) shows the corresponding temporal intensity evolutions measured by the photodetector. Spectral patterns are visible in Fig. 2(a) arising from interference between bound DSs. A noticeable feature is that the patterns evolve over consecutive RTs, indicating moving of the soliton molecules. Such movements are clearly observed in Fig. 2(b), which shows that the separation between the two DSs evolves aperiodically with time, around 60 ps. The energy evolutions are also plotted [Fig. 2(b), the black line], calculated from the spectra. The energy fluctuates significantly once the corresponding spectra broadens (~RTs 500–2500, for instance) and stays quasi-stable when the width of spectra keeps almost invariant (~RTs 2500–5000). The spectral width oscillates slightly before it starts to broaden around a RT number of

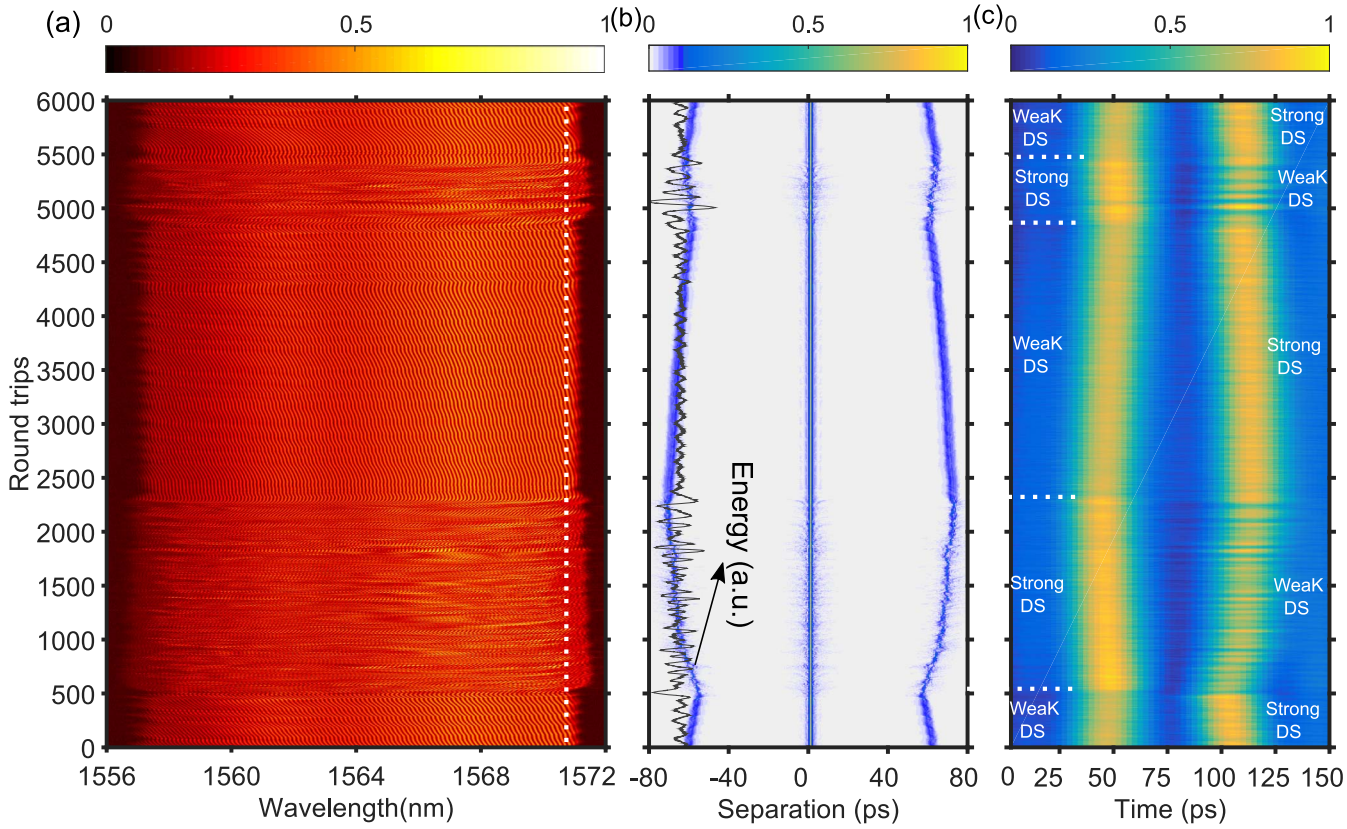

Fig. 2. (a) Real-time spectra evolutions of soliton molecules measured by TS-DFT over 6000 RTs. (b) The field autocorrelation trace calculated from the spectra revealing the temporal dynamics. (c) The corresponding temporal intensity evolutions measured by a photodetector.

500. The spectral width oscillating arises from the energy variation as shown in Fig. 2(b) (the black line). Noisy structures appear on the field autocorrelation traces [Fig. 2(b)] when the spectral width broadens (~RTs 500–2000, 5000-5500). Two cross-sections of the spectra and field autocorrelation traces at RT numbers of 20 and 620 are shown in Fig. 3(a) and 3(b), respectively. The period of the spectral modulation is as small as 0.13 nm at the RT 20 [Fig. 3(a), the red line]. Spectral modulation of 0.13 nm corresponds to two pulses with a separation of 62. 7 ps, which agrees well with that in Fig. 3(b) (the red curve). Such a small spectral modulation (0.13 nm) is beyond the resolution of many TS-DFT systems, which generally have a resolution ranging from 0.27 to 1.3 nm [8,21,28]. Here, by virtue of the state-of-the-art electronic systems (30 ps) and a long piece of specified DCF (1200 ps/nm), our TS-DFT yields a resolution of 0.025 nm, more than an order of magnitude decrement, allowing the detection of small spectral modulations. Additional modulations appear on the spectra with a much larger period around 3 nm [Fig. 3(a), the blue curve], corresponding to 2.7 ps separation between pulses. Such a separation is in good agreement with the separation revealed by the field autocorrelation trace [Fig. 3(b), the blue curve].

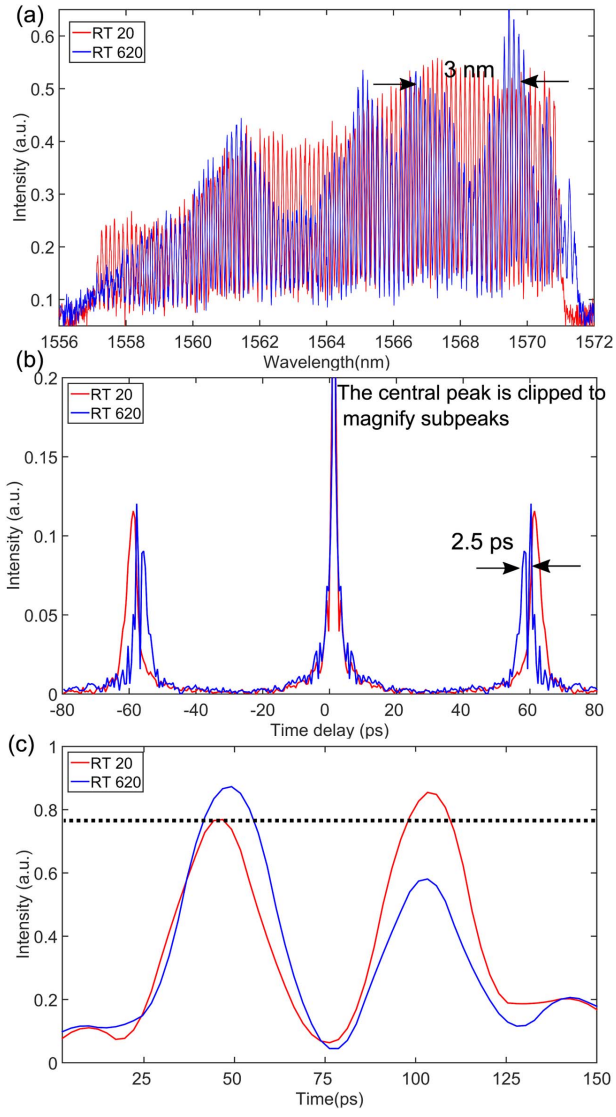

Fig. 3. Two cross-sections of the spectra (a), field autocorrelation traces (b), and temporal intensities (c) at RT numbers of 20 (red) and 620 (blue).

Spatiotemporal intensity measurements provide additional information on the soliton molecule dynamics [Fig. 2(c)]. As seen in the figure, the two DSs have unequal intensities, which is also confirmed by two cross-sections of Fig. 2(c) illustrated in Fig. 3(c). They exchange energy when they collide around a RT number 500, which is also the time when the noise structure appears [Fig. 2(b)]. It is to note that energy-exchange interactions was previously observed between colliding vector solitons [29,30]. The noisy structure indicates either one of the DS splits or both of them split. Figure 2(c) indicates it could be the former: the two pulses have unequal intensities, thus the strong one has a higher possibility to split than the weak one. Figure 2(c) also implies that the large energy fluctuation shown in Fig. 2(b) (~RTs 500–2000) arises from the energy variation of the weak pulse.

The periodical interactions of DSs shown above (Fig. 2) refer to short-range interactions, as the separation between the pulses is only 2.4 times the pulse duration, which is 25 ps measured by an autocorrelator. This interaction scenario resembles that of direct soliton-soliton interactions [31], expect that DS splits and repel each other afterwards.

As the energy varies significantly revealed in Fig. 2(b), it is necessary to investigate the intensity distribution of the spectra. To this end, the intensities of the spectral peaks over 20,000 RTs are used to calculate probability distribution functions (PDFs). The PDF is shown in Fig. 4. The distribution deviates from standard ones given that there are pronounced tails starting from a normalized intensity value of 2.0. Moreover, the tails signature the generation of RWs. Waves having a height larger than twice the significant wave height (SWH) is defined to be RWs [32]. The SWH (the average amplitude of the highest third waves) is 1.7. The intensities larger than 3.4 refer to RWs in Fig. 4. Recently, RWs detected in the spectral domain were coined as spectral RWs [33].

In addition to the soliton molecules described above, another soliton molecule was observed: the spectral patterns evolved while the separation between DSs was fixed as revealed by the field autocorrelation trace. A stationary soliton molecule with fixed separation and phase was not found. The origin is as

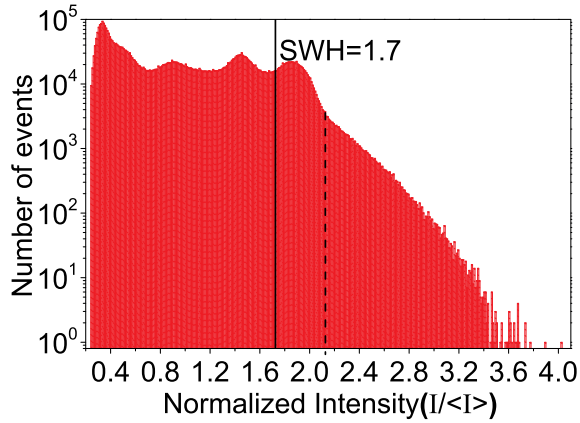

Fig. 4. Spectral intensity histogram of the soliton molecule.

follows. In integrable systems, field overlapping dominates soliton interactions. In these cases, the interaction potential between solitons has no local minima; thus, bound solitons cannot be generated [16]. In dissipative systems, such as lasers, dissipative effects involve in soliton interactions leading to rather different dynamics [34]. In particular, in the anomalous-dispersion regime, mode-locked pulses resemble that of solitons in the sense that the pulses has a sech^2 intensity profile. In this case, dissipative effects such as an output coupler perturbs the solitons, resulting in the emission of dispersive waves. The interference between dispersive waves and solitons generates oscillating structures in the soliton tail. A minimum interaction potential is given by these oscillating tails, and therefore, bound solitons can be formed [16]. However, in the normal-dispersion regime, the pulses generated from a laser is rather different from a soliton. The above-mentioned mechanism for the generation of oscillating structures is absent. Thus, no stationary soliton molecules exist in this case.

In conclusion, we report on the first real-time observation of dynamical soliton molecules in the normal-dispersion regime of a mode-locked fiber laser. DS splitting, rogue wave generation, and energy exchanges are distinct features of soliton molecules in the normal-dispersion regime. Such features could relate to high energies of DSs as well as pronounced dissipative effects, such as gain filtering, since the spectral width of DS approaches that of gain bandwidth of EDF. These soliton molecule dynamics are expected to be discovered in many dissipative systems. Meanwhile, numerical simulations based on the Ginzburg–Landau equation are stimulated by our work to investigate complex dissipative soliton interactions [35].

Funding. National Natural Science Foundation of China (NSFC) (11704123, 61775059); Science and Technology Innovation Program of Basic Science Foundation of Shanghai (18JC1412000); Key Project of Shanghai Education Commission (2017-01-07-00-05-E00021).

REFERENCES

1. K. Goda and B. Jalali, Nat. Photonics **7**, 102 (2013).
2. G. Herink, B. Jalali, C. Ropers, and D. Solli, Nat. Photonics **10**, 321 (2016).
3. P. Ryczkowski, M. Närhi, C. Billet, J. M. Merolla, G. Genty, and J. M. Dudley, Nat. Photonics **12**, 221 (2018).
4. J. Peng, M. Sorokina, S. Sugavanam, N. Tarasov, D. V. Churkin, S. K. Turitsyn, and H. Zeng, Commun. Phys. **1**, 20 (2018).
5. X. Liu and Y. Cui, Adv. Photon. **1**, 016003 (2019).
6. X. Liu, D. Han, Z. Sun, C. Zeng, H. Lu, D. Mao, Y. Cui, and F. Wang, Sci. Rep. **3**, 2718 (2013).
7. G. Herink, F. Kurtz, B. Jalali, D. R. Solli, and C. Ropers, Science **356**, 50 (2017).
8. K. Krupa, K. Nithyanandan, U. Andral, P. Tchofo-Dinda, and P. Grelu, Phys. Rev. Lett. **118**, 243901 (2017).
9. J. Peng and H. Zeng, Laser Photon. Rev. **12**, 1800009 (2018).
10. X. Liu, X. Yao, and Y. Cui, Phys. Rev. Lett. **121**, 023905 (2018).
11. A. Chong, J. Buckley, W. Renninger, and F. Wise, Opt. Express **14**, 10095 (2006).
12. F. W. Wise, A. Chong, and W. H. Renninger, Laser Photon. Rev. **2**, 58 (2008).
13. W. H. Renninger, A. Chong, and F. W. Wise, Opt. Lett. **33**, 3025 (2008).
14. J. Peng, L. Zhan, S. Luo, and Q. S. Shen, IEEE Photon. Technol. Lett. **25**, 948 (2013).
15. A. Zavyalov, R. Iliew, O. Egorov, and F. Lederer, Phys. Rev. A **80**, 043829 (2009).
16. B. A. Malomed, Phys. Rev. A **44**, 6954 (1991).
17. Y. Wang, F. Leo, J. Fatome, M. Erkintalo, S. G. Murdoch, and S. Coen, Optica **4**, 855 (2017).
18. A. F. Runge, N. G. Broderick, and M. Erkintalo, Optica **2**, 36 (2015).
19. K. Krupa, K. Nithyanandan, and P. Grelu, Optica **4**, 1239 (2017).
20. M. Liu, A.-P. Luo, Y.-R. Yan, S. Hu, Y.-C. Liu, H. Cui, Z.-C. Luo, and W.-C. Xu, Opt. Lett. **41**, 1181 (2016).
21. M. Liu, A.-P. Luo, W.-C. Xu, and Z.-C. Luo, Opt. Lett. **41**, 3912 (2016).
22. J. Peng, N. Tarasov, S. Sugavanam, and D. Churkin, Opt. Express **24**, 21256 (2016).
23. Y. Yu, Z.-C. Luo, J. Kang, and K. K. Wong, Opt. Lett. **43**, 4132 (2018).
24. Y. Wei, B. Li, X. Wei, Y. Yu, and K. K. Wong, Appl. Phys. Lett. **112**, 081104 (2018).
25. A. F. Runge, C. Aguergaray, N. G. Broderick, and M. Erkintalo, Opt. Lett. **39**, 319 (2014).
26. Z. Liu, S. Zhang, and F. W. Wise, Opt. Lett. **40**, 1366 (2015).
27. J. Peng and H. Zeng, Phys. Rev. Appl. **11**, 044068 (2019).
28. A. F. Runge, C. Aguergaray, N. G. Broderick, and M. Erkintalo, Opt. Lett. **38**, 4327 (2013).
29. C. Anastassiou, M. Segev, K. Steiglitz, J. Giordmaine, M. Mitchell, M.-F. Shih, S. Lan, and J. Martin, Phys. Rev. Lett. **83**, 2332 (1999).
30. S. Stalin, R. Ramakrishnan, M. Senthilvelan, and M. Lakshmanan, Phys. Rev. Lett. **122**, 043901 (2019).
31. G. P. Agrawal, *Nonlinear Fiber Optics* (Academic, 2007).
32. C. Lecaplain, P. Grelu, J. Soto-Crespo, and N. Akhmediev, Phys. Rev. Lett. **108**, 233901 (2012).
33. C. Lecaplain and P. Grelu, Phys. Rev. A **90**, 013805 (2014).
34. V. V. Afanasjev and N. Akhmediev, Phys. Rev. E **53**, 6471 (1996).
35. N. Akhmediev, J. M. Soto-Crespo, M. Grapinet, and P. Grelu, Opt. Fiber Technol. **11**, 209 (2005).